This is a repository copy of *A New Iron Loss Model for Temperature Dependencies of Hysteresis and Eddy Current Losses in Electrical Machines*.

White Rose Research Online URL for this paper:
http://eprints.whiterose.ac.uk/128254/

Version: Accepted Version

---

**Article:**
Xue, S., Feng, J., Guo, S. et al. (3 more authors) (2018) A New Iron Loss Model for Temperature Dependencies of Hysteresis and Eddy Current Losses in Electrical Machines. IEEE Transactions on Magnetics, 54 (1). 8100310. ISSN 0018-9464

https://doi.org/10.1109/TMAG.2017.2755593

---

**Reuse**
Items deposited in White Rose Research Online are protected by copyright, with all rights reserved unless indicated otherwise. They may be downloaded and/or printed for private study, or other acts as permitted by national copyright laws. The publisher or other rights holders may allow further reproduction and re-use of the full text version. This is indicated by the licence information on the White Rose Research Online record for the item.

**Takedown**
If you consider content in White Rose Research Online to be in breach of UK law, please notify us by emailing eprints@whiterose.ac.uk including the URL of the record and the reason for the withdrawal request.

eprints@whiterose.ac.uk
https://eprints.whiterose.ac.uk/

# A New Iron Loss Model for Temperature Dependencies of Hysteresis and Eddy Current Losses in Electrical Machines

Shaoshen Xue[1], Jianghua Feng[2], Shuying Guo[2], Jun Peng[2], W. Q. Chu[2], and Z.Q. Zhu[1]

[1]Department of Electronic and Electrical Engineering, University of Sheffield, Mappin Street, Sheffield S1 3JD, UK
[2]CRRC Zhuzhou Institute Co. Ltd, Shidai Road, Shifeng District, Zhuzhou, Hunan, 412001, China

**Abstract— In this paper, the different temperature dependencies of hysteresis and eddy current losses of non-oriented Si-steel laminations are investigated. The measured iron loss results show that both the hysteresis and eddy current losses vary linearly with temperature between 40°C to 100°C, a typical temperature range of electrical machines. Varying rates of hysteresis and eddy current losses with the temperature are different and fluctuate with flux density and frequency. Based on this, an improved iron loss model which can consider temperature dependencies of hysteresis and eddy current losses separately is developed. Based on the improved iron loss model, the temperature influence on the iron loss can be fully considered by measuring iron losses at only two different temperatures. The investigation is experimentally validated by both the tests based on a ring specimen and an electrical machine.**

**Index Terms—iron loss, eddy current loss, hysteresis loss, temperature dependency, electrical machines**

.

## I. Introduction

Iron loss is one of the most important design considerations for electrical machines. In order to predict and investigate the iron loss, various iron loss models have been developed, such as the earliest Steinmetz model in [1], three-term models in [2] and [3], as well as two-term models in [4] and [5]. All of them have been used for iron loss investigations. For example, the investigations in [6]-[12] are based on the three-term model in [3] and the investigations in [13]-[19] are based on two-term model in [4]. For electrical machine applications, the two-term models are comparatively more popular mainly due to two facts. First, the classical loss and excess loss in [3] cannot be separated by using Epstein tests [4]. Secondary, the two-term models are easier to implement and having reasonable accuracy. Amongst the two-term models, the model in [5] having variable hysteresis and eddy current loss coefficients has the best accuracy [20]-[22]. However, none of the iron loss model in [1]-[22] considers the influence of temperature.

The iron loss can be influenced by the temperature significantly, such as [23] and [24] on ferrite cores, [25] on NiFe laminations, [26] on oriented silicon laminations, and [27]-[30] on non-oriented silicon laminations. The modeling of temperature influence on iron loss is discussed in [29] and [30]. In [29], only the temperature dependency of the eddy current loss is considered while the hysteresis loss is assumed to be not influenced by the temperature. In [30], the temperature influence on the total iron loss is simply modeled by introducing an equivalent temperature dependent coefficient which is a mix of temperature influences on both the hysteresis and eddy current losses. However in [27] and [28], it has shown experimentally that the hysteresis and eddy current losses have different temperature dependencies.

The aim of this paper is to develop an iron loss model which can consider the temperature dependencies of the hysteresis and the eddy current losses separately. The iron losses at different flux density, frequency and temperature in non-oriented Si-steel laminations are measured firstly by the ring specimen test as will be described in Section II. In Section III, the accuracy of existing iron loss model having variable hysteresis and eddy current loss coefficients but without considering the temperature influence is evaluated first under constant temperature. The influence of temperature on the iron loss and the limitation of the existing model on prediction the iron loss without considering the temperature influence are also demonstrated. In Section IV, the different temperature dependencies of hysteresis and eddy current losses are investigated. An improved iron loss model considering the temperature dependencies of hysteresis and eddy current losses separately is developed and verified by the measured results of ring specimen tests. In Section V, the further experimental validation of the developed iron loss model in an electrical machine is presented.

## II. Iron Loss Measurement of Ring Specimen Made of Silicon Steel Laminations

In this paper, the iron loss investigation is firstly carried out based on the measured results of a ring specimen made of non-oriented silicon steel laminations. The ring specimen iron loss test has been widely used since it is easy to implement and has good accuracy [31]-[36]. The investigation is extended later to the iron loss in an electrical machine.

The ring specimen iron loss measuring system is shown in Fig. 1. The ring specimen has two coils. The excitation coil is supplied by an AC power source. The measuring coil, which has the same number of turns and closely wound together with the excitation coil, is connected to the oscilloscope to measure the instant effective voltage. The instant effective voltage is the voltage on the inductance of the excitation coil. By using the measuring coil, the voltage drop on the excitation coil's resistance can be inherently excluded. The current in the excitation coil is measured by the Tektronix A622 current probe. Thus the iron loss density $p_{\mathrm{Fe}}$ and the field strength H(t) can be calculated as

$$p_{\mathrm{Fe}} = \frac{1}{\rho V}\int_0^T u(t)i(t)\frac{dt}{T} \tag{1}$$

$$H(t) = \frac{Ni(t)}{l_{\mathrm{eff}}} \tag{2}$$

where $p_{\mathrm{Fe}}$ is the iron loss density. $u(t)$ is the instant induced voltage on the measuring coil. $i(t)$ is the instant current in the excitation coil. $T$ is the time period of the current and the voltage. $\rho$ and $V$ are the mass density and the volume of the ring specimen, respectively. $N$ is the number of turns of the excitation coil and the measuring coil. $l_{\mathrm{eff}}$ is the effective length of the ring specimen.

As shown in Table I, the specimen is specially designed to have a big ratio between its average radius and radial thickness. Thus, the flux density can be treated as evenly distributed in the ring specimen and can be calculated as

$$B(t) = \frac{\int u(t)dt}{NA} \tag{3}$$

where $A$ is the cross sectional area of the ring specimen.

Furthermore, iron loss in the ring specimen is utilised to heat the ring specimen to the designate temperature while the temperature is measured by a K-type thermal couple. Thus, iron loss under different temperatures can be obtained. This method has been used in [27] and [28].

All iron losses of the ring specimen are measured when the excitation voltage is sinusoidal. In this case, the input current and hence the voltage drop on the resistance of the excitation coil are not sinusoidal. However, since the voltage drop on the resistance is much smaller compared with the input voltage, u(t) in (3) is only slightly different from sinusoidal. In order to keep u(t) as sinusoidal as possible, the excitation coil is also made of Litz wire with large equivalent cross-section. It is also aimed to reduce the influence of skin and proximity effects at high frequency. The measured resistance of the excitation coil is 0.04 Ω at room temperature. The measured u(t) and input current waveforms are shown in Fig. 2. Thus, the flux density in the ring specimen can also be approximated as sinusoidal according to (3). The test range of the measuring system is summarized in Table II.

The measurement accuracy is very important for this investigation. The measurement accuracy in this paper depends on the accuracy of the current and voltage probes. The current probe Tektronix A622 able to measure current accurately when the current amplitude is as low as 0.05A. The lowest current amplitude during our test is 0.2A at 50Hz and 0.2T. It also able to measure the current up to 2kHz while the maximum frequency of our test is 1kHz. In terms of the voltage probe, Agilent Technologies N2791A differential voltage probe is used in the test. It able to measure voltage accurately when the amplitude is as low as 0.2V. The lowest voltage amplitude during our test is above 2V. Since the thermal time constant is much bigger than the electric time constant for out test rig, the voltage and current can be measured in a very short time before the temperature changes. Hence, the loss at different temperature can be measured accurately. Furthermore, for each set of flux density and frequency, the measurement is repeated several times to reduce the errors as much as possible.

Fig.3 shows the measured B-H loops at 40°C when the frequency is 50Hz and 1000Hz, respectively. It can be seen that the B-H loops will be distorted when the flux density is high due to the saturation at both 50Hz and 1000Hz. The shape of B-H loops, which represents the iron losses in a time period, is frequency and flux density dependent. These dependencies will be discussed later in this paper.

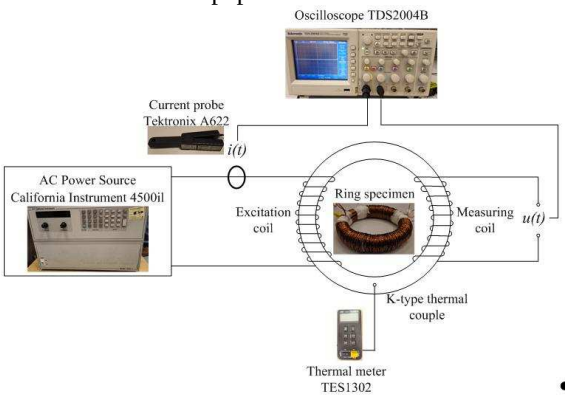


Fig. 1. Schematic diagram of the ring specimen iron loss measuring system.

TABLE I PARAMETERS OF RING SPECIMEN

| | | |
|---|---|---|
| Type of silicon steel laminations | | V300-35A |
| Thickness of single laminations | mm | 0.35 |
| Outer diameter of ring specimen | mm | 150 |
| Inner diameter of ring specimen | mm | 125 |
| Total effective thickness of ring specimen | mm | 14 |
| Number of turns for excitation and measuring coils N | | 102 |

TABLE II TEST RANGE OF RING SPECIMEN IRON LOSS MEASURING SYSTEM

| | | |
|---|---|---|
| Maximum output voltage in RMS value | V | 150 |
| Maximum output current in RMS value | A | 30 |
| Frequency range | Hz | 50-1000 |
| Temperature range | °C | 40-100 |

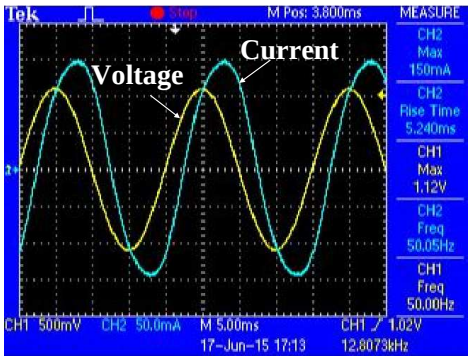


(a)

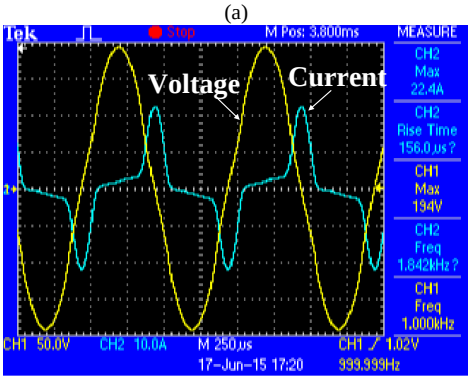


(b)

Fig. 2. Typical waveforms for measured currents of excitation coil and voltages of measuring coil. (a) $B_m$=0.2T and f=50Hz. (b) $B_m$=1.73T and f=1000Hz.

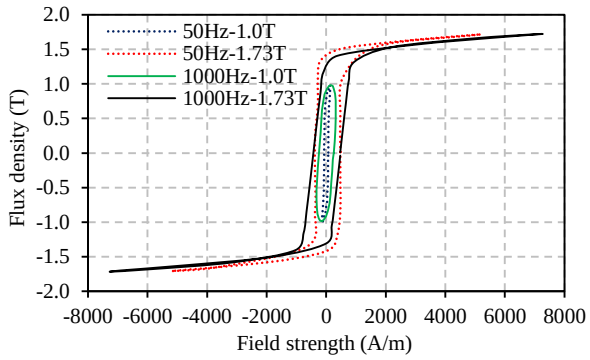


Fig. 3. Measured B-H loops at 40°C when frequency is 50Hz and 1000Hz.

## III. Iron Loss Model without Considering Temperature Influence

According to the review in this paper, the iron loss models developed in [4] and [5] are two of the latest and most widely used models when the flux density is alternating sinusoidally. The comparison between these two models is carried out in [30]. The model developed in [5] is experimentally confirmed to be more accurate with the help of variable coefficients. Therefore, in this paper, the iron loss model developed in [5] is selected for further research. This iron loss model is expressed as:

$$p_{\mathrm{Fe}} = k_{\mathrm{h}}(f, B_{\mathrm{m}}) f B_{\mathrm{m}}^2 + k_{\mathrm{e}}(f, B_{\mathrm{m}}) f^2 B_{\mathrm{m}}^2 \quad (4)$$

where f is the frequency. $B_m$ is the peak value of alternating flux density. $k_{\mathrm{h}}(f, B_{\mathrm{m}})$ and $k_{\mathrm{e}}(f, B_{\mathrm{m}})$ are the hysteresis loss and the eddy current loss coefficients, respectively.

The division of (4) by $f B_{\mathrm{m}}^2$ yields the linear equation below,

$$\frac{p_{\mathrm{Fe}}}{f B_{\mathrm{m}}^2} = k_{\mathrm{h}}(f, B_{\mathrm{m}}) + k_{\mathrm{e}}(f, B_{\mathrm{m}}) f \quad (5)$$

Coefficients $k_{\mathrm{h}}(f, B_{\mathrm{m}})$ and $k_{\mathrm{e}}(f, B_{\mathrm{m}})$ at specific frequency and flux density are identifiable from the y-axis crossing point and the slope of the line. The hysteresis loss and eddy current loss coefficients are then separated. Based on the two measured results having the same flux density and the adjacent frequencies, a set of $k_{\mathrm{h}}(f, B_{\mathrm{m}})$ and $k_{\mathrm{e}}(f, B_{\mathrm{m}})$ can be calculated based on (5). In the similar way, $k_{\mathrm{h}}(f, B_{\mathrm{m}})$ and $k_{\mathrm{e}}(f, B_{\mathrm{m}})$ can be obtained under different flux densities and frequencies using the measured data. Secondly, in order to simplify the modelling of the coefficients, the variation of coefficients with the frequency is considered by using two sets of results representing the low and high frequency regions. In this paper, the low frequency covers 50Hz, 200Hz and 400Hz whilst the high frequency covers 600Hz, 800Hz and 1000Hz. This method is also used in [5].

It should be noted that the temperature influence on iron loss is not considered in this model. The coefficients of this model are obtained based on the measurement iron loss when the temperature is constant. In this paper, all coefficients of this model are obtained when the lamination temperature is 40°C.

Fig. 4 shows the comparison of the predicted iron loss by existing model (4) with the measured iron loss at different lamination temperatures. The existing model (4) is able to accurately predict the iron loss at different flux densities and different frequencies when the lamination temperature remains 40ºC. However, the iron loss could vary significantly when the temperature increases from 40ºC to 100°C, as shown in Fig. 4. However, the predicted iron loss of existing model (4) cannot reflect this variation. Therefore, the prediction accuracies of this existing model can be significantly degraded when the temperature changes.

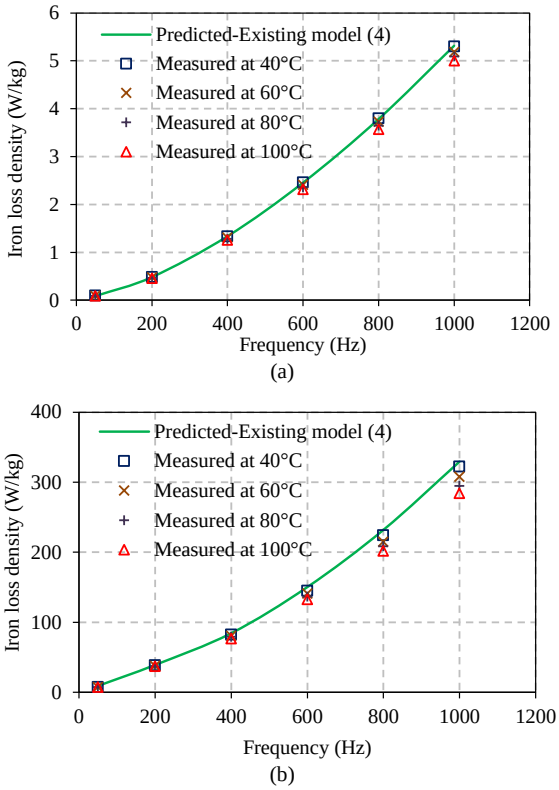


Fig. 4. Measured iron loss and predicted iron loss of existing model (4), (a) $B_m$=0.2T, (b) $B_m$=1.73T.

## IV. Modelling of Temperature Dependencies of Hysteresis Loss and Eddy Current Loss

### A. Improved iron loss model

According to the iron loss model (4), when the frequency f and the flux density $B_m$ are determined, the hysteresis loss and the eddy current loss will be only determined by the coefficients $k_{\mathrm{h}}(f, B_{\mathrm{m}})$ and $k_{\mathrm{e}}(f, B_{\mathrm{m}})$, respectively. Since the flux density and frequency are not temperature dependent, the temperature influence on hysteresis and eddy current losses will be reflected directly by the loss coefficients $k_{\mathrm{h}}(f, B_{\mathrm{m}})$ and $k_{\mathrm{e}}(f, B_{\mathrm{m}})$. Therefore, the investigation on temperature dependencies of hysteresis loss and eddy current loss coefficients is necessary for further modelling.

In order to investigate the temperature dependencies of the hysteresis loss and the eddy current loss separately, the coefficients $k_{\mathrm{h}}(f, B_{\mathrm{m}})$ and $k_{\mathrm{e}}(f, B_{\mathrm{m}})$ in (4) are calculated respectively based on the measured iron loss at different temperatures and shown in Figs. 5 and 6. It can be seen that both the hysteresis loss $k_{\mathrm{h}}(f, B_{\mathrm{m}})$ coefficient and the eddy current loss $k_{\mathrm{e}}(f, B_{\mathrm{m}})$ coefficient vary not only with frequency and flux density but also with temperature. Therefore, the correct iron loss model, which is designated as improved model in this paper, is then developed and can be expressed as:

$$p_{\mathrm{Fe,T}} = k_{\mathrm{h}}(T,f,B_{\mathrm{m}})fB_{\mathrm{m}}^2 + k_{\mathrm{e}}(T,f,B_{\mathrm{m}})f^2B_{\mathrm{m}}^2 \quad (6)$$

where $p_{\mathrm{Fe,T}}$ is the iron loss density at the actual temperature T. $k_{\mathrm{h}}(T,f,B_{\mathrm{m}})$ and $k_{\mathrm{e}}(T,f,B_{\mathrm{m}})$ are hysteresis loss and eddy current loss coefficients, respectively.

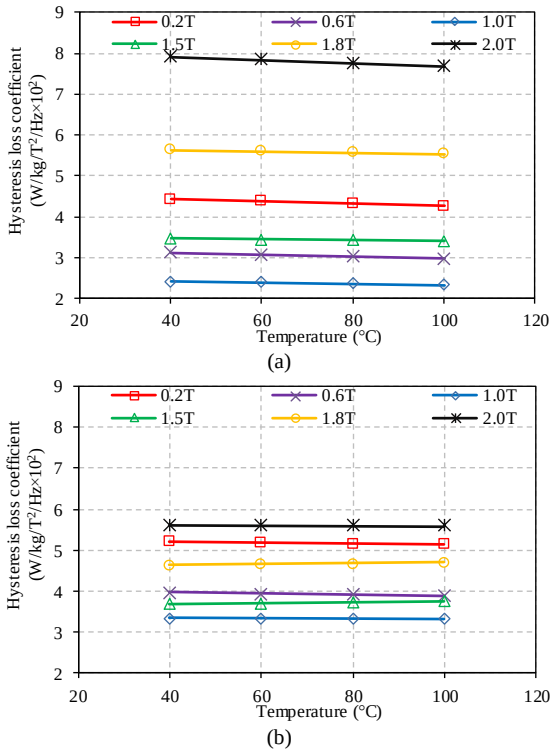


Fig.5. Hysteresis loss coefficient at (a) 50Hz (b) 1000Hz.

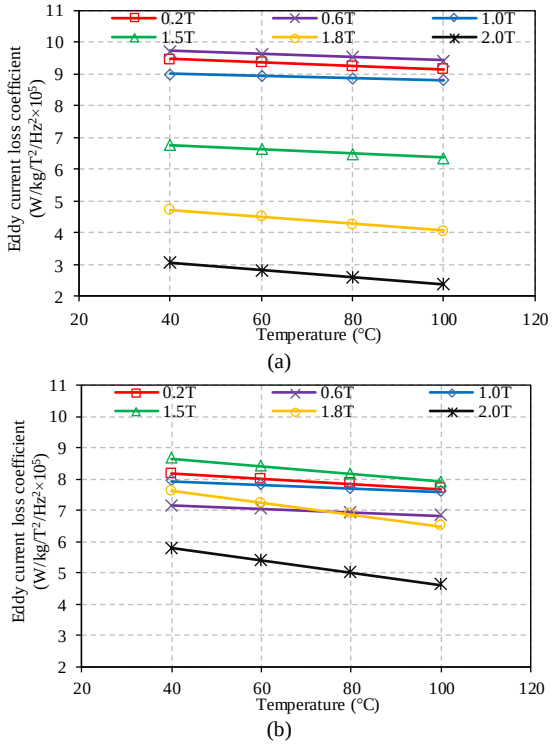


Fig.6. Eddy current loss coefficient at (a) 50Hz (b) 1000Hz.

## B. Modelling of temperature dependent coefficients

According to the improved iron loss model (6), iron loss coefficients at any temperature, frequency and flux density among the test range can be calculated by interpolation $k_{\mathrm{h}}(T,f,B_{\mathrm{m}})$ and $k_{\mathrm{e}}(T,f,B_{\mathrm{m}})$ the coefficient shown in Figs. 5 and 6. The temperature dependency of the iron loss can be then fully considered. However, the coefficients have to be measured at many different temperatures to guarantee the accuracy of the interpolation, which is complicated and time consuming.

Based on Figs. 5 and 6, it can be further seen that both the hysteresis and eddy current loss coefficients vary approximately linearly with temperature although the varying rate changes with flux density and frequency. These linear variations have also been confirmed in [26] and [27]. Nevertheless, the relationship between these losses and temperature will be far away from linear when the temperature is above 200°C [28]. However, electrical machines rarely operate at a temperature higher than 200°C. Therefore, a simple linear relationship between the coefficients and the temperature can be considered for the typical operation temperature range of electrical machines. On the other hand, it should be noted from Figs. 5 and 6 that the varying rates of hysteresis and eddy current loss coefficients with the temperature are different even under the same flux density and frequency. By considering all these aspects, the temperature dependent iron loss coefficients can be modelled as:

$$k_{\mathrm{h}}(T,f,B_{\mathrm{m}}) = k_{\mathrm{th}}(T,f,B_{\mathrm{m}})k_{\mathrm{h,T_0}}(f,B_{\mathrm{m}}) \quad (7)$$

$$k_{\mathrm{e}}(T,f,B_{\mathrm{m}}) = k_{\mathrm{te}}(T,f,B_{\mathrm{m}})k_{\mathrm{e,T_0}}(f,B_{\mathrm{m}}) \quad (8)$$

where $k_{\mathrm{th}}(T,f,B_{\mathrm{m}})$ and $k_{\mathrm{te}}(T,f,B_{\mathrm{m}})$ are the temperature dependent coefficients of hysteresis and eddy current losses. $k_{\mathrm{h,T_0}}(f,B_{\mathrm{m}})$ and $k_{\mathrm{e,T_0}}(f,B_{\mathrm{m}})$ are the hysteresis and eddy current loss coefficients when the temperature is $T_0$.

As demonstrated above, hysteresis and eddy current loss coefficients vary linearly with temperature with different rates. Therefore, the temperature dependent coefficients can be expressed as:

$$k_{\mathrm{th}}(T,f,B_{\mathrm{m}}) = 1 + (T-T_0)D_{\mathrm{hyst}}(f,B_{\mathrm{m}}) \quad (9)$$

$$k_{\mathrm{te}}(T,f,B_{\mathrm{m}}) = 1 + (T-T_0)D_{\mathrm{eddy}}(f,B_{\mathrm{m}}) \quad (10)$$

where $D_{\mathrm{hyst}}(f,B_{\mathrm{m}})$ and $D_{\mathrm{eddy}}(f,B_{\mathrm{m}})$ are varying rates of the hysteresis and eddy current loss coefficients with temperature and can be calculated by measured hysteresis losses and eddy current losses at two different temperatures $T_0$ and $T_1$ for the same frequency and flux density as:

$$D_{\mathrm{hyst}}(f,B_{\mathrm{m}}) = \frac{k_{\mathrm{h,T_1}}(f,B_{\mathrm{m}}) - k_{\mathrm{h,T_0}}(f,B_{\mathrm{m}})}{(T_1-T_0)k_{\mathrm{h,T_0}}(f,B_{\mathrm{m}})} \quad (11)$$

$$D_{\mathrm{eddy}}(f,B_{\mathrm{m}}) = \frac{k_{\mathrm{e,T_1}}(f,B_{\mathrm{m}}) - k_{\mathrm{e,T_0}}(f,B_{\mathrm{m}})}{(T_1-T_0)k_{\mathrm{h,T_0}}(f,B_{\mathrm{m}})} \quad (12)$$

where $k_{\mathrm{h,T_1}}(f,B_{\mathrm{m}})$, $k_{\mathrm{h,T_0}}(f,B_{\mathrm{m}})$, $k_{\mathrm{e,T_1}}(f,B_{\mathrm{m}})$ and $k_{\mathrm{e,T_0}}(f,B_{\mathrm{m}})$ are the hysteresis and eddy current loss coefficients when the temperature is $T_1$ and $T_0$, respectively.

In this paper, $T_1$ is set to 100°C and $T_0$ is set to 40°C. Positive $D_{\mathrm{hyst}}(f,B_{\mathrm{m}})$ or $D_{\mathrm{eddy}}(f,B_{\mathrm{m}})$ means that the loss increases with temperature rise while negative $D_{\mathrm{hyst}}(f,B_{\mathrm{m}})$ or $D_{\mathrm{eddy}}(f,B_{\mathrm{m}})$ means that the loss decreases with temperature

rise. According to (11) and (12), the improved iron loss model has two advantages: First, the temperature dependencies of the hysteresis loss and the eddy current can be considered separately. Second, the temperature influence on the iron loss can be considered by the measured results at only two different temperatures $T_1$ and $T_0$.

In order to investigate the variation of $D_{\mathrm{hyst}}(f, B_{\mathrm{m}})$ and $D_{\mathrm{eddy}}(f, B_{\mathrm{m}})$ with the frequency, the whole frequency test range 50-1000Hz is simply divided into two segments, i.e., the low frequency 50-400Hz and the high frequency 400-1000Hz. Fig. 7 shows the $D_{\mathrm{hyst}}(f, B_{\mathrm{m}})$ and $D_{\mathrm{eddy}}(f, B_{\mathrm{m}})$ at low frequency and high frequency, respectively. By applying $D_{\mathrm{hyst}}(f, B_{\mathrm{m}})$ and $D_{\mathrm{eddy}}(f, B_{\mathrm{m}})$ to (9) and (10) respectively, the temperature dependent coefficients can be then obtained. Fig. 8 shows the predicted temperature dependent coefficients at low frequency and high frequency, respectively. The temperature influences on the iron losses are then considered by substituting these temperature dependent coefficients to (7) and (8).

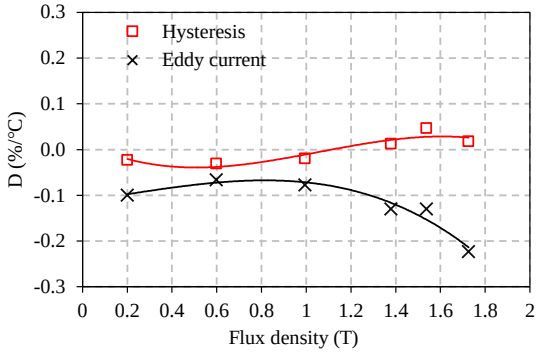


(a)

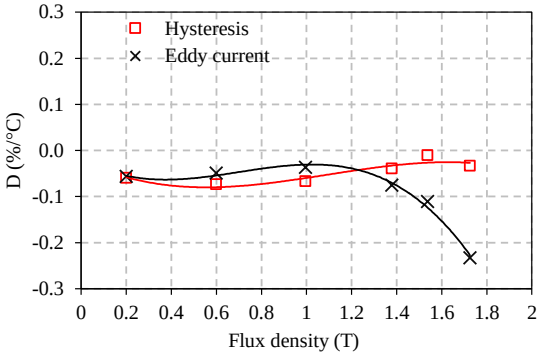


(b)

Fig. 7. Hysteresis loss varying rate $D_{\mathrm{hyst}}$ and eddy current loss varying rate $D_{\mathrm{eddy}}$. (a) low frequency (50-400Hz), (b) high frequency (400-1000Hz).

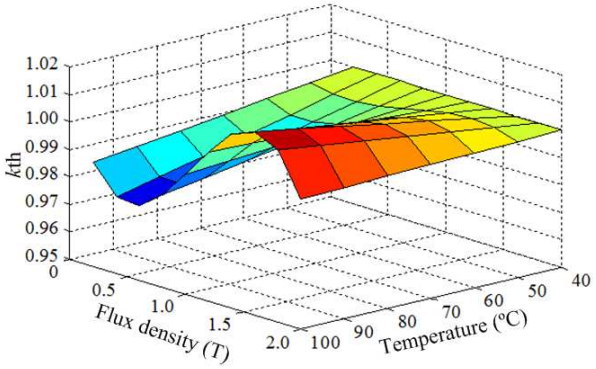


(a)

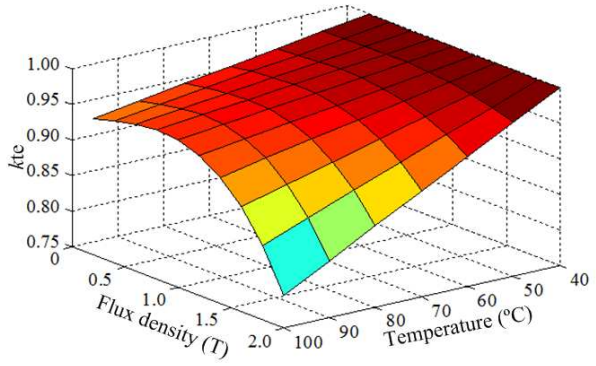


(b)

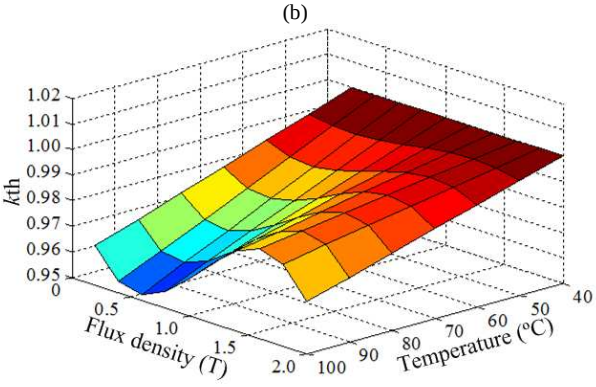


(c)

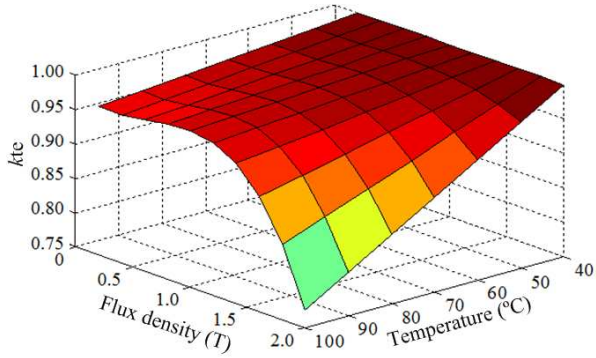


(d)

Fig. 8. Predicted temperature dependent coefficients of hysteresis loss and eddy current loss, (a) $k_{\mathrm{th}}$ in low frequency (50-400Hz), (b) $k_{\mathrm{te}}$ in low frequency (50-400Hz), (c) $k_{\mathrm{th}}$ in high frequency (400-1000Hz), (d) $k_{\mathrm{te}}$ in high frequency (400-1000Hz).

## C. Validation of improved iron loss model

Fig. 9 shows the measured and predicted iron loss at different frequency and flux density when the temperature is 100°C. It can be seen that when the temperature changes to 100°C, the improved model can track the variation of iron loss more precisely. In order to compare the predicted and measured iron losses more clearly and comprehensively, the relative prediction error is employed,

$$\mathrm{err} = (p_{\mathrm{Fe,Pre}} - p_{\mathrm{Fe,Mea}})/p_{\mathrm{Fe,Mea}} \tag{13}$$

where err is the relative prediction error. $p_{\mathrm{Fe,Pre}}$ is the predicted iron loss density. $p_{\mathrm{Fe,Mea}}$ is the measured iron loss density.

With the help of the relative prediction error, it is much easier to show whether the influence of temperature is considered effectively or not. The variation of the relative

prediction error with the temperature will be stable and stay low if the influence of temperature is considered effectively.

Fig. 10 shows the comparison of relative prediction errors of existing and improved models at different flux density, frequency and temperature. It can be seen that the relative prediction errors of existing model (4) vary significantly with the temperature rise. This is due to the fact that the existing model (4) cannot reflect the temperature influence on iron losses. The prediction iron losses of the existing model keep constant while the actual iron losses vary significantly when temperature changes. On the other hand, the improved model (6) can predict the iron losses with low and stable relative prediction errors even when the temperature changes significantly. This is due to the fact that the improved model (6) can track the iron loss variation with temperature. This means that the improved model can consider the temperature influence on iron losses effectively.

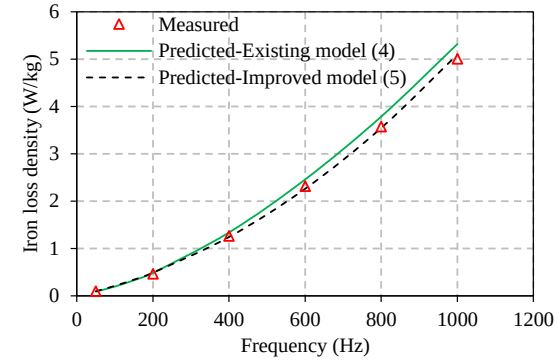


(a)

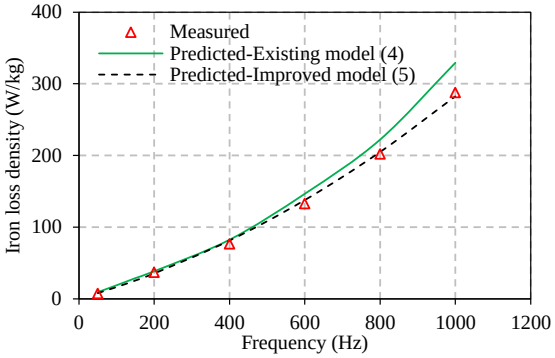


(b)

Fig. 9. Predicted and measured iron loss at different frequency and flux density when the temperature is 100ºC, (a) $B_m$=0.2T, (b) $B_m$=1.73T.

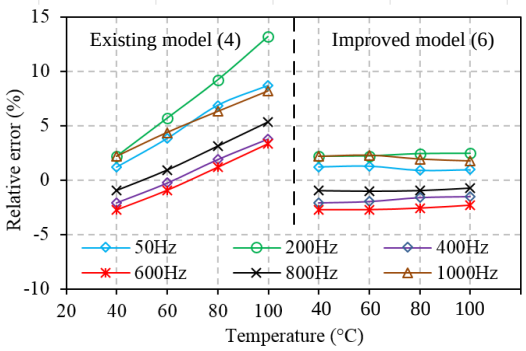


(a)

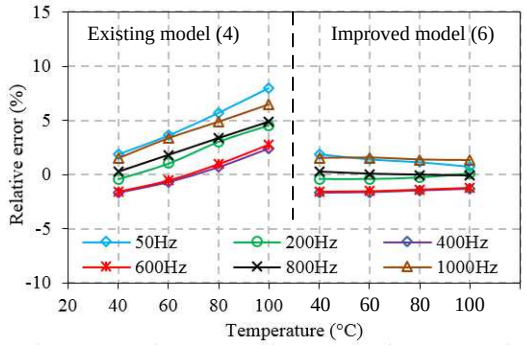


(b)

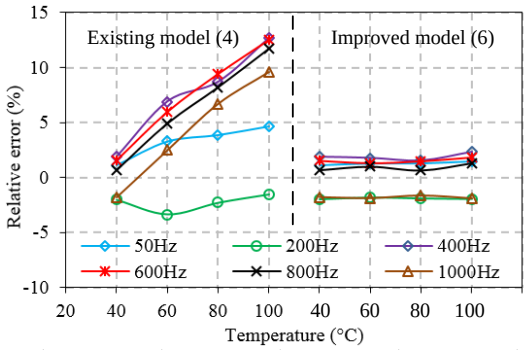


(c)

Fig. 10. Relative prediction errors of existing and improved models, (a) $B_m$=0.2T, (b) $B_m$=1.0T, (c) $B_m$=1.73T

## V. Further Experimental Validation in an Electrical Machine

In the previous sessions, the accuracy of the improved iron loss model on predicting the iron loss considering temperature influence has been validated by the measured results of ring specimen test. However, the flux density distribution and variation in electrical machines are uneven and much more complicated than the ones in the ring specimen. Therefore, it is important to evaluate the accuracy of the improved model in real electrical machines, which is carried out in this section.

The measuring system of iron loss in an electrical machine under different flux density, frequency and temperature is shown in Fig. 11. A 12/10 IPM machine is employed for the test. In order to remove the mechanical loss and the magnet eddy current loss, the machine rotor is locked and there is no magnet in the rotor. The three-phase windings are powered by the three-phase AC power source. The measured iron loss of the electrical machine can be obtained by subtracting the copper loss from the total loss.

$$P_{\mathrm{Fe}} = P_{\mathrm{in}} - P_{\mathrm{Cu}} \tag{14}$$

where $P_{\mathrm{Fe}}$ is the total iron loss of the electrical machine. $P_{\mathrm{in}}$ is the input power to the machine. $P_{\mathrm{Cu}}$ is the copper loss, which can be calculated by the measured winding resistance considering temperature dependency.

In order to measure the temperatures of different parts of the electrical machine, six thermal couples are installed at the stator yoke, the coil, the stator tooth, the tooth tip, the rotor magnet slot and the rotor yoke as it shown in Fig. 12. The electrical machine is heated to the target temperature by its own losses. Fig. 13 shows the temperature variation in different parts of the electrical machine when the phase current is 2.16A and 3.11A

at 1000Hz, respectively. It can be seen that after two hours heating on the machine, the heat transfer is almost completed and the temperatures of different parts tend to be stable. When the phase current is 2.16A, 1000Hz, the hottest part is the coil (71ºC) and the coolest part is the rotor yoke (68ºC) after 120 mins heating. The temperature difference between different parts is very small and the average temperature of different part is 69ºC. In this circumstance, the temperature of the electrical machine can be approximately considered as 69ºC. On the other hand, when the phase current is 3.11A, 1000Hz, the hottest part is the coil (103ºC) and the coolest part is the stator yoke (99ºC) after 120 mins heating, the average temperature of different part is 100ºC. The temperature of the electrical machine can be approximately considered as 100ºC In order to ensure the thermal transferring is completed for each test, the machine is heated to the designated temperature by a long-term heating. Then, the losses are measured by applying the pre-tuned input. Since the measuring process will only take a few seconds, the temperature variation during the measurement can be neglected. The iron losses under different currents at 69ºC and 100ºC can be obtained by repeating the foregoing process.

To predict the iron loss, the electrical machine is modelled in the FEA software with the measured phase current waveforms shown in Fig. 14. Fig. 15 shows the simulated flux density distribution by FEA when the phase current $I_a$=0A, $I_b$=6.12A, $I_c$=-6.12A. Then, the iron loss is predicted from flux density variations in each FE element using the improved iron loss model. It should be noticed that the flux density in the electrical machine can be rotational. The rotational flux density is decomposed into two alternating directions, i.e. the major-axis and the minor-axis as shown in Fig. 16. The major-axis is aligned with the long side of the rotational flux density while the minor-axis is aligned with the short side of the rotational flux density. The iron loss in each alternating direction can be calculated, respectively. The total iron loss under rotational flux density can be then obtained by the sum of iron losses at these two directions. The temperature dependent losses coefficients for the core are obtained by the ring specimen tests using the same lamination. The measured and predicted iron losses of the electrical machine are compared to evaluate the model accuracy.

Fig. 17 shows measured and predicted results at 69ºC and 100°C. The numerical results are listed in Table III in Appendix. It can be seen that when the temperature rises to 69ºC and 100ºC, the improved model (6) can reflect the variation of the iron loss while the existing model (4) cannot. The accuracy of the improved model (6) is therefore much better than that of the existing model (4) with the help of temperature dependent coefficients. The effectiveness of the improved model on iron loss prediction in the electrical machine is then confirmed.

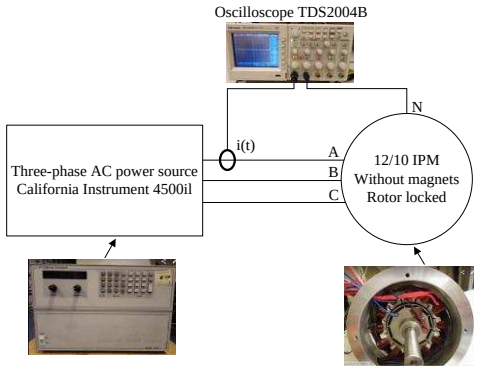


Fig. 11. Locked rotor test without magnets.

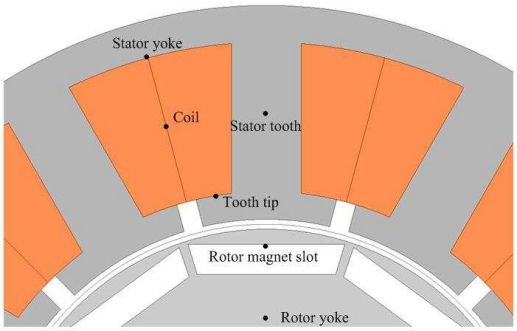


Fig. 12. Thermal couples in the electrical machine.

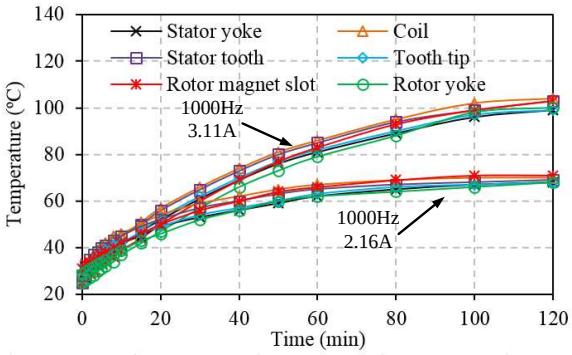


Fig. 13. Temperature variation of different parts of electrical machine when supplied by different phase currents.

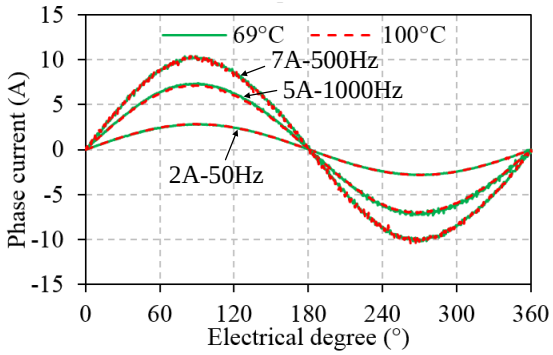


Fig. 14. Measured phase current waveforms when temperature is 69°C and 100°C at different frequencies.

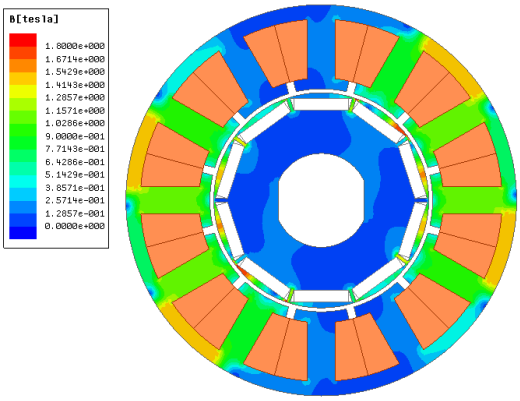


Fig. 15. FEA simulated flux-density distribution when $I_a$=0A, $I_b$=6.12A, $I_c$=-6.12A has been added to Section V, Fig. 15.

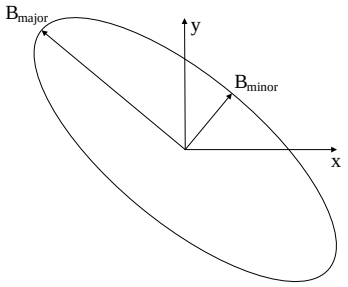


Fig. 16. Major and minor axes of the rotational flux density in electrical machines.

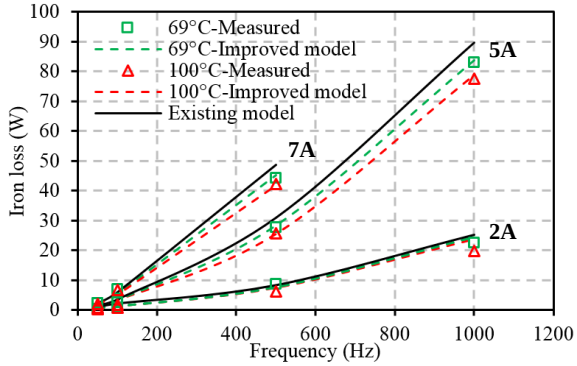


Fig. 17. Measured and predicted results of electrical machine when the temperature is 69ºC and 100ºC.

## VI. Conclusions

In this paper, different temperature influences on hysteresis and eddy current losses of non-oriented Si-steel laminations are investigated. It is found that both the hysteresis and eddy current losses vary with the temperature. An improved iron loss model considering temperature dependencies of the hysteresis loss and the eddy current loss separately is developed. It is also found that the variations of hysteresis and eddy current losses with temperature is almost linear for the typical operation range of electrical machines although the varying rate of hysteresis and eddy current losses are different. Based on these linear relationships, a simplified modelling method of the temperature dependent loss coefficients is also proposed. Using the improved model, the temperature influence on iron loss can be fully considered by simply measured results at two different temperatures. The investigation is experimentally validated by both the lamination ring specimen test and the lock rotor no-PM electrical machine test. This iron loss model could be useful for electromagnetic-thermal coupled analyses to predict the iron loss as well as the temperature distribution in electrical machines. These modelling and electromagnetic-thermal coupled analyses will be carried out in the future.

## References

[1] C. P. Steinmetz, “On the law of hysteresis,” Trans. Amer. Inst. Elect. Eng., vol. 9, no. 1, pp. 3-64, 1892, Jan. 1892.

[2] R. H. Pry and C. P. Bean, “Calculation of the energy loss in magnetic sheet materials using a domain model,” J. Appl. Phys., vol. 29, no. 3, pp. 532-533, Mar. 1958.

[3] G. Bertotti, “General properties of power losses in soft ferromagnetic materials,” IEEE Trans. Magn., vol. 24, no. 1, pp. 621-630, Jan. 1988.

[4] A. Boglietti, A. Cavagnino, M. Lazzari, and M. Pastorelli, “Predicting iron losses in soft magnetic materials with arbitrary voltage supply: an engineering approach,” IEEE Trans. Magn., vol. 39, no. 2, pp. 981-989, Mar. 2003.

[5] D. M. Ionel, M. Popescu, M. I. McGilp, T. J. E. Miller, S. J. Dellinger, and R. J. Heideman, “Computation of core losses in electrical machines using improved models for laminated steel,” IEEE Trans. Ind. Appl., vol. 43, no. 6, pp. 1554-1564, Nov./Dec. 2007.

[6] F. Fiorillo and A. Novikov, “An improved approach to power losses in magnetic laminations under nonsinusoidal induction wave-form,” IEEE Trans. Magn., vol. 26, no. 5, pp. 2904-2910, Sep. 1990.

[7] K. Atallah, Z. Q. Zhu, and D. Howe, “An improved method for predicting iron losses in brushless permanent-magnet DC drives,” IEEE Trans. Magn., vol. 28, no. 5, pp. 2997-2999, Sep. 1992.

[8] A. Hemeida and P. Sergeant, “Analytical modeling of surface PMSM using a combined solution of Maxwell’s equations and magnetic equivalent circuit,” IEEE Trans. Magn., vol. 50, no. 12, pp. 1-13, Dec. 2014.

[9] O. de la Barriere, C. Appino, F. Fiorillo, C. Ragusa, M. Lecrivain, L. Rocchino, H. Ben Ahmed, M. Gabsi, F. Mazaleyrat, and M. LoBue, “Characterization and prediction of magnetic losses in soft magnetic composites under distorted induction waveform,” IEEE Trans. Magn., vol. 49, no. 4, pp. 1318-1326, Apr. 2013.

[10] B. Zhang, R. Qu, J. Wang, J. Li, W. Xu, and Y. Chen, “Electromagnetic-thermal coupling analysis of permanent magnet synchronous machines for electric vehicle applications based on improved (μ+1) evolution strategy,” IEEE Trans. Magn., vol. 51, no. 4, pp.1-10, Apr. 2015.

[11] M. Cossale, A. Krings, J. Soulard, A. Boglietti, and A. Cavagnino, “Practical investigations on cobalt-iron laminations for electrical machines,” IEEE Trans. Ind. Appl., vol. PP, no. 99, pp. 1, Jan. 2015.

[12] A. Krings, S. Nategh, O. Wallmark, and J. Soulard, “Influence of the welding process on the performance of slotless PM motors with SiFe and NiFe stator laminations,” IEEE Trans. Ind. Appl., vol. 50, no. 1, pp. 296-306, Jan./Feb. 2014.

[13] S. Zhu, M. Cheng, J. N. Dong, and J. Du, “Core loss analysis and calculation of stator permanent-magnet machine considering dc-biased magnetic induction,” IEEE Trans. Ind. Electron, vol. 61, no. 10, pp. 5203-5212, Oct. 2014.

[14] J. Seo, S. Kwak, S. Jung, C.-G. Lee, T.-K. Chung, and H.-K. Jung, “A research on iron loss of IPMSM with a frictional number of slot per pole,” IEEE Trans. Magn., vol. 45, no. 3, pp. 1824-1827, Mar. 2009.

[15] T. Taitoda, Y. Takahashi, and K. Fujiwara, “Iron loss estimation method for a general hysteresis loop with minor loops,” IEEE Trans. Magn., in press.

[16] H. Domeki, Y. Ishihara, C. Kaido, Y. Kawase, S. Kitamura, T. Shimomura, N. Takahashi, T. Yamada, and K. Yamazaki, “Investigation of benchmark model for estimating iron loss in rotating machine,” IEEE Trans. Magn., vol. 40, no. 2, pp. 794-797, Mar. 2004.

[17] K. Yamazaki and W. Fukushima, “Loss analysis of induction motors by considering shrink fitting of stator housings,” IEEE Trans. Magn., vol. 51, no. 3, Mar. 2015.

[18] R. Akaki, Y. Takahashi, K. Fujiwara, M. Matsushita, N. Takahashi, and M. Morita, “Effect of magnetic property in bridge area of IPM motors on torque characteristics,” IEEE Trans. Magn., vol. 49, no.5, pp. 2335-2338, May. 2013.

[19] K. Yamazaki and Y. Kanou, "Shape optimization of rotating machines using time-stepping adaptive finite element method," IEEE Trans. Magn., vol. 46, no. 8, pp. 3113-3116, Aug. 2010.
[20] A. Boglietti, A. Cavagnino, D. M. Ionel, M. Popescu, D. A. Staton, and S. Vaschetto, "A general model to predict the iron losses in PWM inverter-fed induction motors," IEEE Trans. Ind. Appl., vol. 46, no. 5, pp. 1882-1890, Sep./Oct. 2010.
[21] M. Popescu, D. M. Ionel, A. Boglietti, A. Cavagnino, C. Cossar, and M. I. McGilp, "A general model for estimating the laminated steel losses under PWM voltage supply," IEEE Trans. Ind. Appl., vol. 46, no. 4, pp. 1389-1396, Jul./Aug. 2010.
[22] C. Wooyoung, L. Silong, and B. Sarlioglu, "Core loss estimation of high speed electric machines: An assessment," in IEEE Ind. Electron. Society 39th Annu. Conf., Vienna, Austria, Nov. 2013, pp. 2691-2696.
[23] P. R.Wilson, J. N. Ross, and A. D. Brown, "Simulation of magnetic component models in electric circuits including dynamic thermal effects," IEEE Trans. Power Electron., vol. 17, no. 1, pp. 55-65, Jan. 2002.
[24] A. Raghunathan, Y. Melikhov, J. Snyder, and D. Jiles, "Modeling the temperature dependence of hysteresis based on Jiles-Atherton theory," IEEE Trans. Magn., vol. 45, no. 10, pp. 3954-3957, Oct. 2009.
[25] A. Krings, S. A. Mousavi, O. Wallmark, and J. Soulard, "Temperature influence of NiFe steel laminations on the characteristics of small slotless permanent magnet machines," IEEE Trans. Magn., vol. 49, no. 7, pp. 4064-4067, Jul. 2013.
[26] K. Foster, "Temperature-Dependence of Loss Separation Measurements for Oriented Silicon Steels," IEEE Trans. Magn., vol. 22, no. 1, pp. 49-53, Jan. 1986.
[27] N. Takahashi, M. Morishita, D. Miyagi, and M. Nakano, "Examination of magnetic properties of magnetic materials at high temperature using a ring specimen," IEEE Trans. Magn., vol. 46, no. 2, pp. 548-551, Feb. 2010.
[28] N. Takahashi, M. Morishita, D. Miyagi, and M. Nakano, "Comparison of Magnetic Properties of Magnetic Materials at High Temperature," IEEE Trans. Magn., vol. 47, pp. 4352-4355, Oct. 2011.
[29] J. Chen, D. Wang, S. Cheng, Y. Wang, Y. Zhu, and Q. Liu, "Modeling of temperature effects on magnetic property of non-oriented silicon steel lamination", IEEE Trans. Magn., in press.
[30] S. Xue, W. Q. Chu, Z. Q. Zhu, J. Peng, S. Guo, J. Feng, "Iron loss calculation considering temperature influence in non-oriented steel laminations", in IET Sci. Meas. Technol. vol. 10, no. 8 pp. 846-854, Nov. 2016.
[31] A. Boglietti, A. Cavagnino, L. Ferraris, and M. Lazzari, "The annealing influence onto the magnetic and energetic properties in soft magnetic material after punching process," in IEEE Electric Mach. and Drives, Madison, USA, Jun. 2003, pp. 503-508.
[32] A. Moses and S. Hamadeh, "Comparison of the Epstein-square and a single-strip tester for measuring the power loss of nonoriented electrical steels," IEEE Trans. Magn., vol. 19, no. 6, pp. 2705-2710, Nov. 1983.
[33] A. Espíndola, F. Tristão, J. P. Schlegel, N. J. Batistela, N. Sadowski, P. Kuo-Peng, M. Rigoni, "Comparison of iron losses evaluations by different testing procedures," in Elect. Mach. 2010 XIX Int. Conf., Rome, Italy, Sept. 2010, pp. 1-4.
[34] A. Krings and J. Soulard, "Experimental characterization of magnetic materials for electrical machine applications," in IEEE Elect. Mach. Design, Control and Diagnosis Workshop, Torino, Italy, Mar. 2015, pp. 85-89.
[35] J. Muhlethaler, J. Biela, J. W. Kolar, and A. Ecklebe, "Core losses under the DC bias condition based on Steimetz parameters," IEEE Trans. Power Electron., vol. 27, no. 2, pp. 953-963, Feb. 2012.
[36] L. K. Rodrigues and G. W. Jewell, "Model specific characterization of soft magnetic materials for core loss prediction in electrical machines," IEEE Trans. Magn., vol. 50, no. 11, pp. 1-4, Nov. 2014.
[37] M. Enokizono, T. Suzuki, J. Sievert, and J. Xu, "Rotational power loss of silicon steel sheet," IEEE Trans. Magn., vol. 26, no. 5, pp. 2562-2564, Sep. 1990.
[38] J. G. Zhu and V. S. Ramsden, "Improved formulations for rotational core losses in rotating electrical machines," IEEE Trans. Magn., vol. 34, no. 4, pp. 2234-2242, Jul. 1998.
[39] Y. G. Guo, J. G. Zhu., J. Zhong, H. Lu, and J. X. Jin, "Measurement and modeling of rotational core losses of soft magnetic materials used in electrical machines: A review," IEEE Trans. Magn., vol. 44, no. 2, pp. 279-291, Feb. 2008.
[40] K. Yamazaki, Y. Fukushima, and M. Sato, "Loss analysis of permanent-magnet motors with concentrated windings-variation of magnet eddy-current loss due to stator and rotor shapes," IEEE Trans. Ind. Appl., vol. 45, no. 4, pp. 1334-1342, Jul./Aug. 2009.
[41] S. Calverley, G. Jewell, and R. Saunders, "Prediction and measurement of core losses in a high-speed switched-reluctance machine," IEEE Trans. Magn., vol. 41, no. 11, pp. 4288-4298, Nov. 2005.

## APPENDIX

TABLE III MEASURED AND PREDICTED RESULTS

| | | 2A | 5A | 7A |
|---|---|---|---|---|
| **50Hz** | **69°C** | | | |
| | Measured (W) | 0.30 | 1.20 | 2.12 |
| | Existing model (W) | 0.73 | 1.55 | 2.20 |
| | Improved model (W) | 0.72 | 1.51 | 2.13 |
| | **100°C** | | | |
| | Measured (W)(Variation compare to 69°C) | 0.28 (-6.0%) | 1.18 (-1.6%) | 1.99 (-6.2%) |
| | Existing model (W) | 0.73 | 1.55 | 2.20 |
| | Improved model (W) (Variation compare to 69°C) | 0.71 (-1.4%) | 1.48 (-2.1%) | 2.06 (-3.3%) |
| **100Hz** | **69°C** | | | |
| | Measured (W) | 0.77 | 2.59 | 6.95 |
| | Existing model (W) | 1.23 | 3.42 | 5.62 |
| | Improved model (W) | 1.21 | 3.34 | 5.41 |
| | **100°C** | | | |
| | Measured (W) (Variation compare to 69°C) | 0.68 (-11%) | 2.39 (-7.7%) | 6.81 (-1.9%) |
| | Existing model (W) | 1.23 | 3.42 | 5.62 |
| | Improved model (W) (Variation compare to 69°C) | 1.19 (-1.7%) | 3.27 (-1.9%) | 5.20 (-3.9%) |
| **500Hz** | **69°C** | | | |
| | Measured (W) | 7.64 | 27.8 | 44.3 |
| | Existing model (W) | 7.36 | 30.1 | 48.4 |
| | Improved model (W) | 7.15 | 28.4 | 45.6 |
| | **100°C** | | | |
| | Measured (W) (Variation compare to 69°C) | 6.68 (-12%) | 25.7 (-7.6%) | 42.3 (-4.6%) |

| | | | | |
|---|---|---|---|---|
| | Existing model (W) | 7.36 | 30.1 | 48.4 |
| | Improved model (W) (Variation compare to 69°C) | 6.94 (-2.9%) | 26.7 (-5.9%) | 42.8 (-6.2%) |
| **1000Hz** | **69°C** | | | |
| | Measured (W) | 22.1 | 83.0 | |
| | Existing model (W) | 25.2 | 88.9 | |
| | Improved model (W) | 24.4 | 83.9 | |
| | **100°C** | | | |
| | Measured (W) (Variation compare to 69°C) | 19.9 (-10%) | 77.6 (-6.6%) | |
| | Existing model (W) | 25.2 | 88.9 | |
| | Improved model (W) (Variation compare to 69°C) | 23.7 (-2.9%) | 78.8 (-6.0%) | |